Supplementary Materials for *Similarity solutions and regularisation of inertial surfactant dynamics*

Jun Eshima[1], Luc Deike[1,2], and Howard A. Stone[1]

[1]Department of Mechanical and Aerospace Engineering, Princeton University, Princeton, New Jersey 08544, USA
[2]High Meadows Environmental Institute, Princeton University, Princeton, New Jersey 08544, USA

This supplementary material contains the details of the numerical schemes used in obtaining solutions of the thin film equations considered in the main text. The structure of the supplementary material is as follows. Section 1 describes the numerical scheme for the IM regime, section 2 describes the numerical scheme for the IMC regime, section 3 describes the numerical scheme for the IME regime, and section 4 describes the numerical scheme for the IMCE regime.

1 Numerical scheme for the IM regime thin film equations

In this section, the numerical scheme for the IM regime is given. Throughout the text, a Gaussian initial condition is considered. In other words, we numerically solve

$$\frac{\partial u}{\partial t} = -u\frac{\partial u}{\partial r} + \frac{2\sigma'(\Gamma)}{h}\frac{\partial \Gamma}{\partial r}, \tag{1a}$$

$$\frac{\partial h}{\partial t} = -\frac{1}{r}\frac{\partial}{\partial r}\left(ruh\right), \tag{1b}$$

$$\frac{\partial \Gamma}{\partial t} = -\frac{1}{r}\frac{\partial}{\partial r}\left(ru\Gamma\right). \tag{1c}$$

with initial condition

$$u = 0,\ h = 1,\ \Gamma = e^{-r^2} \text{ at } t = 0, \tag{2}$$

boundary conditions

$$u = 0,\ \frac{\partial h}{\partial r} = 0,\ \frac{\partial \Gamma}{\partial r} = 0 \text{ at } r = 0, \tag{3}$$

and undisturbed far field condition

$$u = 0,\ h = 1,\ \Gamma = 0 \text{ at } r = \infty. \tag{4}$$

1.1 Numerical scheme

1.1.1 Choice of spatial grid

The grid was taken to be $[0, L]$ with $L = 5$, which can be seen to be sufficiently wide by seeing the plots of u, h, Γ (such as figure 3 in the main text). Since a shock forms in finite time, there needs to be high resolution in space (and time) as the singularity is approached. Then, the usual course of action would be to consider an adaptive spatial mesh. However, in order to do self-similarity analysis,

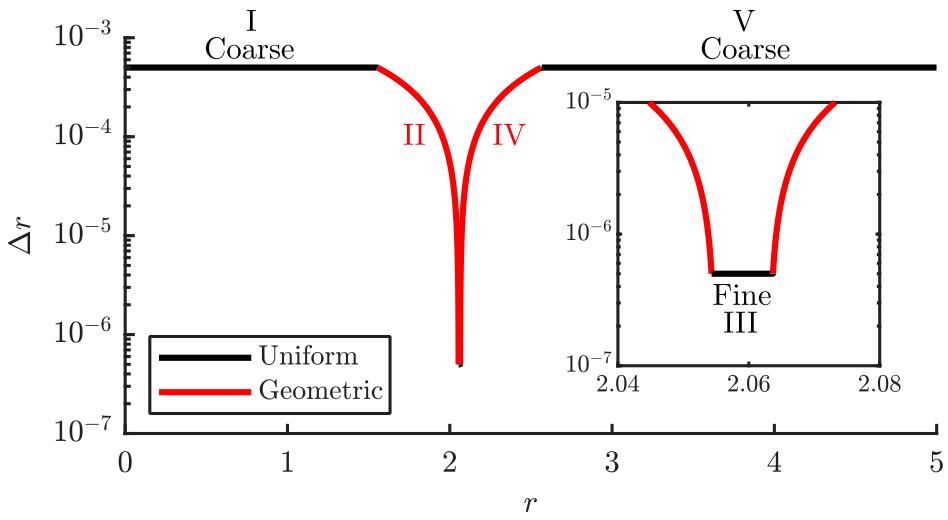

Figure 1: Example of grid with parameters (Δr_0, Δr_1, λ, W)=(5×10^{-7}, 5×10^{-4}, 1.001, 0.005), centered about $r_c = 2.06$. The difference between gridpoints Δr is plotted against r, where uniform regions are shown in black curves and non-uniform region (geometric regions) shown in red curves. Inset: Magnified view of the coarse region. Regions I, II, III, IV, V are labelled.

the singularity values $t_*, r_*, u_*, h_*, \Gamma_*$ (values of t, r, u, h, Γ at the singularity) need to be determined accurately via interpolation (see section 1.2), but adaptive spatial mesh approaches were found to induce too much oscillation. Then, the next optimal grid choice was to consider a fixed but non-uniform grid. Intuitively, the grid is taken to be refined close to r_* and coarse away from r_*. In the coarsening/refining process, it was found advantageous to change the grid width smoothly to reduce noise in predicting the singularity values. In the region of coarsening/refining, the grid widths between adjacent grids was changed by a factor λ (λ taken to be suitably close to 1). Of course, in order to create such fixed but non-uniform grids, we need to roughly know where r_* is, such that the grid may be created around it. A reasonable guess for r_* may be obtained by considering a low-resolution uniform grid set up. In the particular set of equations above (1,2,3,4), $r_* \approx 2.06 =: r_c$ may be obtained cheaply from such uniform grids. Then, the grid is constructed using four parameters $\Delta r_0, \Delta r_1, \lambda, W$ as follows (an example of the grid is shown in Figure 1):

- (Uniform fine region) the interval $[r_c - W, r_c + W]$ is uniform with spatial resolution Δr_0 [region III].
- (Geometric region) Going right from $r = r_c + W$, let the grid spacings be $\lambda \Delta r_0, \lambda^2 \Delta r_0, \cdots \lambda^n \Delta r_0$, where n is chosen such that $\Delta r_1 \approx \lambda^n \Delta r_0$ [region IV]. Go left from $r = r_c - W$ in an analogous way [region II].
- (Uniform coarse region) Once resolution Δr_1 is reached, the grid is kept uniform [regions I,V].

1.1.2 Choice of numerical solver

In order to obtain second order convergence in space and time, the Crank-Nicolson method (implicit) was taken with centered finite difference. At the left boundary ($r = 0$), Dirichlet condition was used to set $u = 0$, Neumann conditions were used to set $\frac{\partial h}{\partial r} = \frac{\partial \Gamma}{\partial r} = 0$. At the right boundary ($r = 5$), Neumann conditions were used to set $\frac{\partial u}{\partial r} = \frac{\partial h}{\partial r} = \frac{\partial \Gamma}{\partial r} = 0$. The discretisation is explicitly given by

(where X_i^m denotes variable X at the ith grid point r_i at the mth time step):

$$\begin{aligned}
u_i^{m+1} &= u_i^m + \frac{\Delta t}{2}\left(-u_i^{m+1}\frac{u_{i+1}^{m+1}-u_{i-1}^{m+1}}{(r_{i+1}-r_{i-1})} - \frac{2}{h_i^{m+1}}\frac{\Gamma_{i+1}^{m+1}-\Gamma_{i-1}^{m+1}}{(r_{i+1}-r_{i-1})}\right) \\
&\quad + \frac{\Delta t}{2}\left(-u_i^{m}\frac{u_{i+1}^{m}-u_{i-1}^{m}}{(r_{i+1}-r_{i-1})} - \frac{2}{h_i^{m}}\frac{\Gamma_{i+1}^{m}-\Gamma_{i-1}^{m}}{(r_{i+1}-r_{i-1})}\right) \qquad (5a) \\
h_i^{m+1} &= h_i^m + \frac{\Delta t}{2}\left(-\frac{u_i^{m+1}h_i^{m+1}}{r_i} - u_i^{m+1}\frac{h_{i+1}^{m+1}-h_{i-1}^{m+1}}{(r_{i+1}-r_{i-1})} - h_i^{m+1}\frac{u_{i+1}^{m+1}-u_{i-1}^{m+1}}{(r_{i+1}-r_{i-1})}\right) \\
&\quad + \frac{\Delta t}{2}\left(-\frac{u_i^{m}h_i^{m}}{r_i} - u_i^{m}\frac{h_{i+1}^{m}-h_{i-1}^{m}}{(r_{i+1}-r_{i-1})} - h_i^{m}\frac{u_{i+1}^{m}-u_{i-1}^{m}}{(r_{i+1}-r_{i-1})}\right) \qquad (5b) \\
\Gamma_i^{m+1} &= \Gamma_i^m + \frac{\Delta t}{2}\left(-\frac{u_i^{m+1}\Gamma_i^{m+1}}{r_i} - u_i^{m+1}\frac{\Gamma_{i+1}^{m+1}-\Gamma_{i-1}^{m+1}}{(r_{i+1}-r_{i-1})} - \Gamma_i^{m+1}\frac{u_{i+1}^{m+1}-u_{i-1}^{m+1}}{(r_{i+1}-r_{i-1})}\right) \\
&\quad + \frac{\Delta t}{2}\left(-\frac{u_i^{m}\Gamma_i^{m}}{r_i} - u_i^{m}\frac{\Gamma_{i+1}^{m}-\Gamma_{i-1}^{m}}{(r_{i+1}-r_{i-1})} - \Gamma_i^{m}\frac{u_{i+1}^{m}-u_{i-1}^{m}}{(r_{i+1}-r_{i-1})}\right) \qquad (5c)
\end{aligned}$$

The values $((u_i^{m+1})_{i=1,\ldots,N}, (h_i^{m+1})_{i=1,\ldots,N}, (\Gamma_i^{m+1})_{i=1,\ldots,N}))$ can be obtained from $((u_i^m)_{i=1,\ldots,N}, (h_i^m)_{i=1,\ldots,N}, (\Gamma_i^m)_{i=1,\ldots,N}))$ using Newton Raphson iteration so that (5) is satisfied. In other words, move all the terms in (5) to the left and we numerically solve for

$$\mathbf{F}((u_i^{m+1})_{i=1,\ldots,N}, (h_i^{m+1})_{i=1,\ldots,N}, (\Gamma_i^{m+1})_{i=1,\ldots,N}), (u_i^m)_{i=1,\ldots,N}, (h_i^m)_{i=1,\ldots,N}, (\Gamma_i^m)_{i=1,\ldots,N})) = \mathbf{0} \quad (6)$$

where $\mathbf{F}$ is a $3N$ dimensional vector (each dimension corresponds to one of (5)).

1.1.3 Adaptive time algorithm

An adaptive time algorithm is chosen so that the time resolution can be taken to be finer when needed. The criterion used to give an adaptive time algorithm is by setting an error threshold e_{tol} for the first iteration of the Newton-Raphson iteration. The first guess for $((u_i^{m+1})_{i=1,\ldots,N}, (h_i^{m+1})_{i=1,\ldots,N}, (\Gamma_i^{m+1})_{i=1,\ldots,N}))$ is set to be $((u_i^m)_{i=1,\ldots,N}, (h_i^m)_{i=1,\ldots,N}, (\Gamma_i^m)_{i=1,\ldots,N}))$. More specifically, if

$$\max_i |F_i((u_i^m)_{i=1,\ldots,N}, (h_i^m)_{i=1,\ldots,N}, (\Gamma_i^m)_{i=1,\ldots,N}), (u_i^m)_{i=1,\ldots,N}, (h_i^m)_{i=1,\ldots,N}, (\Gamma_i^m)_{i=1,\ldots,N}))| > e_{\text{tol}}, \quad (7)$$

then the timestep Δt is halved. Intuitively, the criterion (7) ensures that the system does not vary too much in one timestep. If $\Delta t < \Delta t_{\min}$, then the timestep is no longer refined.

1.1.4 Summary of parameters for numerics

There are 6 parameters in total (four spatial, two temporal). These are summarised in Table 1.

Parameter	Description
Δr_0	Spatial resolution of the uniform fine region [section 1.1.1]
Δr_1	Spatial resolution of the uniform coarse region [section 1.1.1]
λ	Geometric factor in the region where coarsening/refining occurs ($\Delta r_{i+1} = \lambda^{\pm 1} \Delta r_i$) [see section 1.1.1]
W	Width of the uniform fine region [section 1.1.1]
e_{tol}	Error threshold for adaptive time algorithm [section 1.1.3]
Δt_{min}	Minimum timestep for adaptive time algorithm [section 1.1.3]

Table 1: Summary of parameters for the numerical scheme for the IM regime

1.2 Systematic derivation of values at singularity

The values $u_*, h_*, \Gamma_*, r_*, t_*$ (values of u, h, Γ, r, t at singularity) must be interpolated from the numerical data. Such a systematic derivation is described below. For this subsection, all the figures shown use the base case parameter for $\sigma(\Gamma) = -\Gamma$. The same method is used for the different isotherms $\sigma(\Gamma)$ considered in this paper (see section 1.3).

As can be seen from the main text, we have

$$\left(\min \frac{\partial u}{\partial r}\right)^{-1} = \left(1 - \frac{\sigma''(\Gamma_*)(\Gamma_*)^2}{h_* V^2}\right)(t - t_*) \tag{8}$$

as $t \to t_*$. Indeed, figure 2(a) plots $(\min \frac{\partial u}{\partial r})^{-1}$ against t close to t_* (black solid curve) and it is seen that indeed, the curve is a straight line until the numerics cannot capture the similarity solution accurately. By increasing the resolution of the simulation, the curve will be straight for further times close to t_*. The value $t_* \approx 1.1364$ can then be obtained by interpolation from the straight line region. As shown in figure 2(a), a best fit straight line of the region where the curve $\left(\min \frac{\partial u}{\partial r}\right)^{-1}$ is straight (red dotted line) is extrapolated to give an estimate for t_* (red dot). Using this estimate for t_*, we may give an estimate for r_* (the location of the shock), by tracking the approach of the inflection point ($\arg\min \frac{\partial u}{\partial r}$) as $t_* - t \to 0^+$ (see figure 2(b)). Similarly, to get an estimate for the values (u_*, h_*, Γ_*) at the shock location, the values of (u, h, Γ) at the inflection point ($\arg\min \frac{\partial u}{\partial r}$) are tracked as $t_* - t \to 0^+$ (see figure 2(c)). For numerical convergence of the interpolated values, see section 1.3.

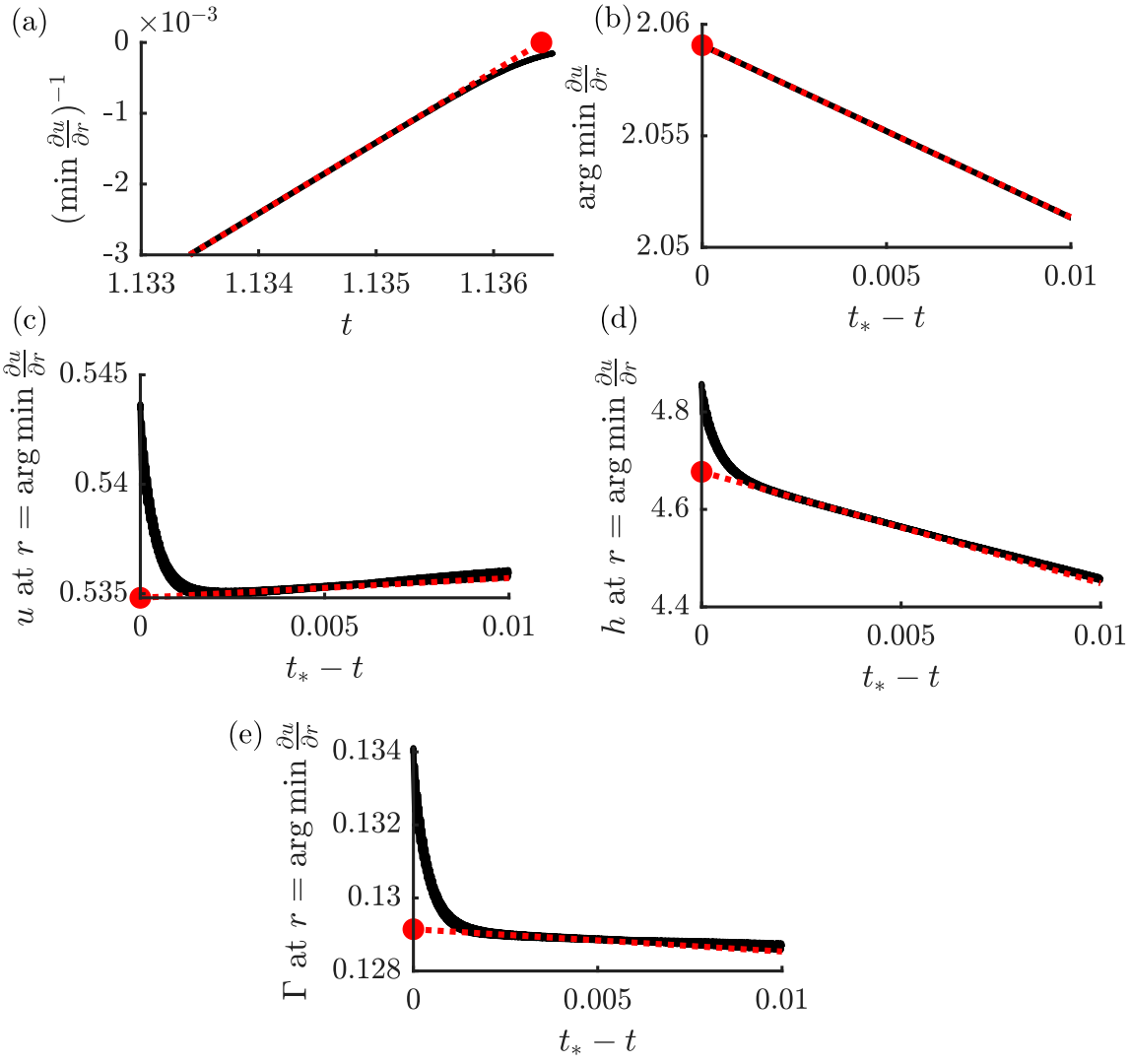

Figure 2: Systematic derivation of singularity variables via interpolation of numerical data (the example $\sigma(\Gamma) = -\Gamma$ is shown). Black curves denote the numerical data and red dotted line and dots shows the interpolation. (a) Plot of $(\min \frac{\partial u}{\partial r})^{-1}$ against t to find the singularity time t_* via interpolation. (b) Plot of $\arg\min \frac{\partial u}{\partial r}$ against $t_* - t$ to find the singularity spatial location r_* via interpolation. (c,d,e) Plot of u, h, Γ at $\arg\min \frac{\partial u}{\partial r}$ to find the singularity values $(u_*, h_*, \Gamma_*) = (u(r_*, t_*), h(r_*, t_*), \Gamma(r_*, t_*))$ via interpolation.

1.3 Numerical convergence

Whenever a new example is considered, one must make sure that the estimated values $u_*, h_*, \Gamma_*, r_*, t_*$ have converged with respect to the simulation parameters shown in Table 1. In this paper, three examples are considered: Linear isotherm $\sigma(\Gamma) = -\Gamma$, concave isotherm $\sigma(\Gamma) = \Gamma_\infty \log\left(1 - \frac{\Gamma}{\Gamma_\infty}\right)$, convex isotherm $\sigma(\Gamma) = -\Gamma_0 \tanh\left(\frac{\Gamma}{\Gamma_0}\right)$ (in particular, $\Gamma_\infty = 1.1$, $\Gamma_0 = 0.1$ are considered). For each of these examples, we show that there is convergence.

1.3.1 Linear isotherm convergence

The isotherm $\sigma(\Gamma) = -\Gamma$ is considered. The following 7 cases are considered. The base case parameters are taken for data shown in the main paper and the 6 other cases correspond to refining the 6 parameters appearing in the simulation (see table 1). All the simulations took under 50 CPU hours on a single core.

- Base: $\Delta r_0 = 5 \times 10^{-7}$, $\Delta r_1 = 5 \times 10^{-4}$, $\lambda = 1.001$, $W = 0.005$, $e_{\text{tol}} = 10^{-3}$, $\Delta t_{\min} = 2 \times 10^{-8}$.
- Δr_0: $\Delta r_0 = 2.5 \times 10^{-7}$, $\Delta r_1 = 5 \times 10^{-4}$, $\lambda = 1.001$, $W = 0.005$, $e_{\text{tol}} = 10^{-3}$, $\Delta t_{\min} = 2 \times 10^{-8}$.
- Δr_1: $\Delta r_0 = 5 \times 10^{-7}$,$\Delta r_1 = 2.5 \times 10^{-4}$, $\lambda = 1.001$,$W = 0.005$,$e_{\text{tol}} = 10^{-3}$, $\Delta t_{\min} = 2 \times 10^{-8}$.
- $\Delta t_{\min}$: $\Delta r_0 = 5 \times 10^{-7}$, $\Delta r_1 = 5 \times 10^{-4}$, $\lambda = 1.001$, $W = 0.005$, $e_{\text{tol}} = 10^{-3}$, $\Delta t_{\min} = 10^{-8}$.
- e_{tol}: $\Delta r_0 = 5 \times 10^{-7}$, $\Delta r_1 = 5 \times 10^{-4}$, $\lambda = 1.001$, $W = 0.005$, $e_{\text{tol}} = 5 \times 10^{-4}$, $\Delta t_{\min} = 2 \times 10^{-8}$.
- λ: $\Delta r_0 = 5 \times 10^{-7}$, $\Delta r_1 = 5 \times 10^{-4}$, $\lambda = 1.0005$, $W = 0.005$, $e_{\text{tol}} = 10^{-3}$, $\Delta t_{\min} = 2 \times 10^{-8}$.
- W: $\Delta r_0 = 5 \times 10^{-7}$, $\Delta r_1 = 5 \times 10^{-4}$, $\lambda = 1.001$,$W = 0.01$, $e_{\text{tol}} = 10^{-3}$, $\Delta t_{\min} = 2 \times 10^{-8}$.

Table 2 shows the convergence of the singularity values $u_*, h_*, \Gamma_*, r_*, t_*$. For concreteness, we mention that when doing the interpolation step from the numerical data, we considered $t = 1.133$ to $t = 1.134$ as being straight line regions, capturing the self similar solution (see section 1.2).

	Base	Δr_0	Δr_1	$\Delta t_{\min}$	e_{tol}	λ	W
t_*	1.1364	1.1364	1.1364	1.1364	1.1364	1.1364	1.1364
r_*	2.0591	2.0591	2.0591	2.0591	2.0591	2.0590	2.0591
u_*	0.5348	0.5347	0.5348	0.5348	0.5348	0.5346	0.5346
h_*	4.6771	4.6748	4.6768	4.6771	4.6770	4.6725	4.6734
Γ_*	0.1291	0.1291	0.1291	0.1291	0.1291	0.1290	0.1290

Table 2: The linear isotherm $\sigma(\Gamma) = -\Gamma$ is considered. Convergence check for the estimated singularity values $u_*, h_*, \Gamma_*, r_*, t_*$ (interpolating from 1.133 to 1.134). Along with the base case, the 6 different cases correspond to refining the 6 parameters appearing in the simulation (see table 1).

Also, we may now show that indeed, the numerical resolution is the reason behind why the relationship $\max\left|\frac{\partial u}{\partial r}\right| \sim (t_* - t)^{-1}$ is eventually not followed as $t \to t_*$. Figure 3 plots $\max\left|\frac{\partial u}{\partial r}\right|$ against $t_* - t$ for the 7 different cases (shown by different greyscales, solid or dashed curves). Recall that the analytical prediction is given by $\max\left|\frac{\partial u}{\partial r}\right| = \left(1 - \frac{\sigma'(\Gamma_*)(\Gamma_*)^2}{h_* V^2}\right)(t_* - t)^{-1}$ (black dotted line). As can be seen, the case Δr_0 (dashed line for clarity), which increases spatial resolution near the shock point, allows the numerics to follow the relation predicted by the analytical prediction closer as $t_* - t \to 0^+$.

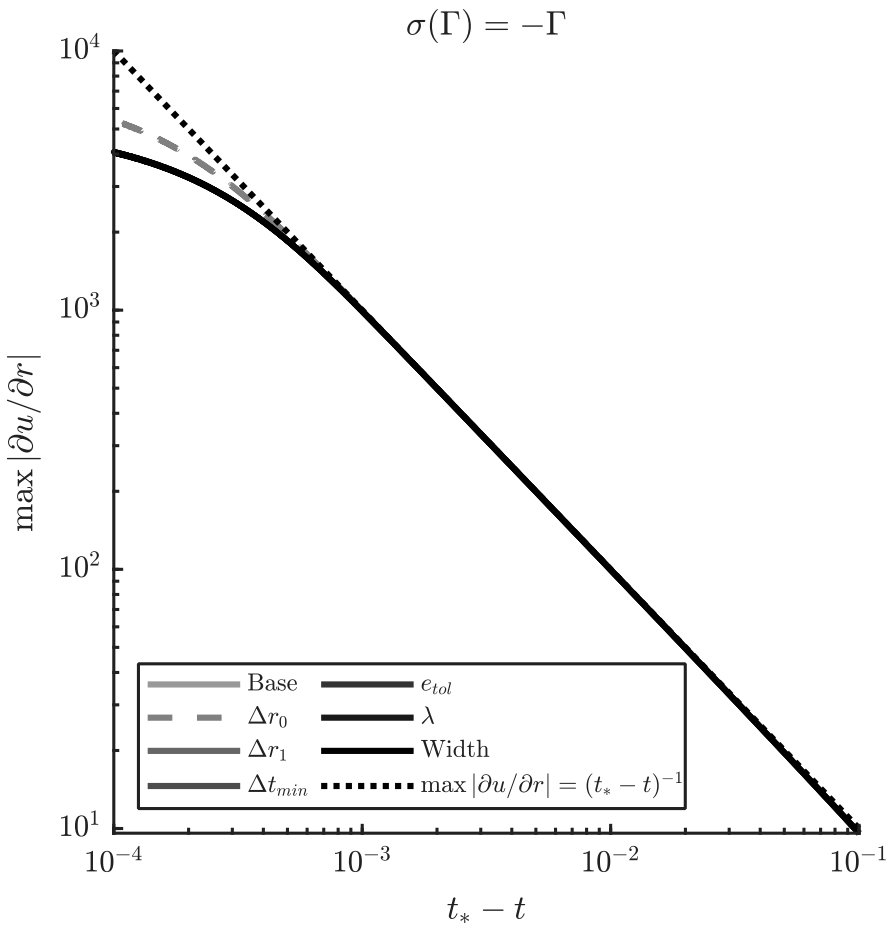

Figure 3: Comparison of different cases of simulation parameters. Plot is $\max\left|\frac{\partial u}{\partial r}\right|$ against $t_* - t$. Solid and dashed lines represent the numerics from the 7 different cases described in the text (Δr_0 case is given as a dashed line to highlight the case). The dotted line is the analytical prediction. The agreement between the numerics and analytical prediction becomes better as numerical resolution is increased (Δr_0 case).

1.3.2 Concave isotherm

The isotherm $\sigma(\Gamma) = \Gamma_\infty \log\left(1 - \frac{\Gamma}{\Gamma_\infty}\right)$ for $\Gamma_\infty = 1.1$ is considered. The cases considered are the same as section 1.3.1. All the simulations took under 25 CPU hours on a single core. In other words,

- Base: $\Delta r_0 = 5 \times 10^{-7}$, $\Delta r_1 = 5 \times 10^{-4}$, $\lambda = 1.001$, $W = 0.005$, $e_{\text{tol}} = 10^{-3}$, $\Delta t_{\min} = 2 \times 10^{-8}$.
- Δr_0: $\Delta r_0 = 2.5 \times 10^{-7}$, $\Delta r_1 = 5 \times 10^{-4}$, $\lambda = 1.001$, $W = 0.005$, $e_{\text{tol}} = 10^{-3}$, $\Delta t_{\min} = 2 \times 10^{-8}$.
- Δr_1: $\Delta r_0 = 5 \times 10^{-7}$,$\Delta r_1 = 2.5 \times 10^{-4}$, $\lambda = 1.001$,$W = 0.005$,$e_{\text{tol}} = 10^{-3}$, $\Delta t_{\min} = 2 \times 10^{-8}$.
- $\Delta t_{\min}$: $\Delta r_0 = 5 \times 10^{-7}$, $\Delta r_1 = 5 \times 10^{-4}$, $\lambda = 1.001$, $W = 0.005$, $e_{\text{tol}} = 10^{-3}$, $\Delta t_{\min} = 10^{-8}$.
- e_{tol}: $\Delta r_0 = 5 \times 10^{-7}$, $\Delta r_1 = 5 \times 10^{-4}$, $\lambda = 1.001$, $W = 0.005$, $e_{\text{tol}} = 5 \times 10^{-4}$, $\Delta t_{\min} = 2 \times 10^{-8}$.
- λ: $\Delta r_0 = 5 \times 10^{-7}$, $\Delta r_1 = 5 \times 10^{-4}$, $\lambda = 1.0005$, $W = 0.005$, $e_{\text{tol}} = 10^{-3}$, $\Delta t_{\min} = 2 \times 10^{-8}$.
- W: $\Delta r_0 = 5 \times 10^{-7}$, $\Delta r_1 = 5 \times 10^{-4}$, $\lambda = 1.001$,$W = 0.01$, $e_{\text{tol}} = 10^{-3}$, $\Delta t_{\min} = 2 \times 10^{-8}$.

Table 3 shows the convergence of the singularity values $u_*, h_*, \Gamma_*, r_*, t_*$. For interpolation step from the numerical data, we considered $t = 0.642$ to $t = 0.643$ as being straight line regions, capturing the self similar solution (see section 1.2).

	Base	Δr_0	Δr_1	$\Delta t_{\min}$	e_{tol}	λ	W
t_*	0.6456	0.6456	0.6456	0.6456	0.6456	0.6454	0.6455
r_*	1.6691	1.6691	1.6691	1.6691	1.6691	1.6689	1.6690
u_*	0.8674	0.8673	0.8674	0.8674	0.8673	0.8664	0.8665
h_*	2.7417	2.7413	2.7413	2.7417	2.7414	2.7349	2.7364
Γ_*	0.2935	0.2935	0.2935	0.2935	0.2935	0.2930	0.2930

Table 3: The concave isotherm $\sigma(\Gamma) = \Gamma_\infty \log\left(1 - \frac{\Gamma}{\Gamma_\infty}\right)$ for $\Gamma_\infty = 1.1$ is considered. Convergence check for the estimated singularity values $u_*, h_*, \Gamma_*, r_*, t_*$ (interpolating from 0.642 to 0.643). Along with the base case, the 6 different cases correspond to refining the 6 parameters appearing in the simulation (see table 1).

1.3.3 Convex isotherm

The isotherm $\sigma(\Gamma) = -\Gamma_0 \tanh\left(\frac{\Gamma}{\Gamma_0}\right)$ for $\Gamma_0 = 0.1$ is considered. The cases are similar to that seen in sections 1.3.1 and 1.3.2, but with a smaller Δr_0 (and a higher e_{tol} to help save CPU costs), which happened to be needed to capture the self similarity nature of the numerical solution as $t \to t_*^-$ upto the same level (around $t_* - t = 10^{-3}$) as for the linear and concave cases. All the simulations took under 70 CPU hours on a single core.

- Base: $\Delta r_0 = 10^{-7}$, $\Delta r_1 = 5 \times 10^{-4}$, $\lambda = 1.001$, $W = 0.005$, $e_{\text{tol}} = 2 \times 10^{-3}$, $\Delta t_{\min} = 2 \times 10^{-8}$.
- Δr_0: $\Delta r_0 = 510^{-8}$, $\Delta r_1 = 5 \times 10^{-4}$, $\lambda = 1.001$, $W = 0.005$, $e_{\text{tol}} = 2 \times 10^{-3}$, $\Delta t_{\min} = 2 \times 10^{-8}$.
- Δr_1: $\Delta r_0 = 10^{-7}$,$\Delta r_1 = 2.5 \times 10^{-4}$, $\lambda = 1.001$,$W = 0.005$,$e_{\text{tol}} = 2 \times 10^{-3}$, $\Delta t_{\min} = 2 \times 10^{-8}$.
- $\Delta t_{\min}$: $\Delta r_0 = 10^{-7}$, $\Delta r_1 = 5 \times 10^{-4}$, $\lambda = 1.001$, $W = 0.005$, $e_{\text{tol}} = 2 \times 10^{-3}$, $\Delta t_{\min} = 10^{-8}$.
- e_{tol}: $\Delta r_0 = 10^{-7}$, $\Delta r_1 = 5 \times 10^{-4}$, $\lambda = 1.001$, $W = 0.005$, $e_{\text{tol}} = 10^{-3}$, $\Delta t_{\min} = 2 \times 10^{-8}$.
- λ: $\Delta r_0 = 10^{-7}$, $\Delta r_1 = 5 \times 10^{-4}$, $\lambda = 1.0005$, $W = 0.005$, $e_{\text{tol}} = 2 \times 10^{-3}$, $\Delta t_{\min} = 2 \times 10^{-8}$.
- W: $\Delta r_0 = 10^{-7}$, $\Delta r_1 = 5 \times 10^{-4}$, $\lambda = 1.001$,$W = 0.01$, $e_{\text{tol}} = 2 \times 10^{-3}$, $\Delta t_{\min} = 2 \times 10^{-8}$.

Table 4 shows the convergence of the singularity values $u_*, h_*, \Gamma_*, r_*, t_*$. Interpolation was from $t = 2.163$ to $t = 2.164$ (see section 1.2).

	Base	Δr_0	Δr_1	$\Delta t_{\min}$	e_{tol}	λ	width
t_*	2.1665	2.1665	2.1665	2.1665	2.1664	2.1664	2.1665
r_*	2.4482	2.4482	2.4482	2.4482	2.4482	2.4482	2.4482
u_*	0.1921	0.1921	0.1921	0.1921	0.1921	0.1920	0.1920
h_*	4.0540	4.0526	4.0535	4.0540	4.0531	4.0504	4.0511
Γ_*	0.0175	0.0175	0.0175	0.0175	0.0175	0.0175	0.0175

Table 4: The convex isotherm $\sigma(\Gamma) = -\Gamma_0 \tanh\left(\frac{\Gamma}{\Gamma_0}\right)$ for $\Gamma_0 = 0.1$ is considered. Convergence check for the estimated singularity values $u_*, h_*, \Gamma_*, r_*, t_*$ (interpolating from 2.163 to 2.164). Along with the base case, the 6 different cases correspond to refining the 6 parameters appearing in the simulation (see table 1)

2 Numerical scheme for the IMC regime thin film equations

The IMC regime was analysed by Eshima et al. [2], where the numerical scheme consisted of a Crank-Nicolson method with centered finite difference (i.e., analgous to (5) but with a capillary pressure term). A uniform grid was used. A sponge layer was used to avoid spurious reflections from the boundaries of the computational domain. For details, see [2].

The IMC equations computed were

$$\frac{\partial u}{\partial t} = -u\frac{\partial u}{\partial r} - \frac{2}{h}\frac{\partial \Gamma}{\partial r} + \frac{1}{2\mathcal{M}}\frac{\partial}{\partial r}\left(\frac{1}{r}\frac{\partial}{\partial r}\left(r\frac{\partial h}{\partial r}\right)\right), \tag{9a}$$

$$\frac{\partial h}{\partial t} = -\frac{1}{r}\frac{\partial}{\partial r}\left(ruh\right), \tag{9b}$$

$$\frac{\partial \Gamma}{\partial t} = -\frac{1}{r}\frac{\partial}{\partial r}\left(ru\Gamma\right). \tag{9c}$$

The initial condition is

$$u = 0,\ h = 1,\ \Gamma = e^{-r^2} \text{ at } t = 0, \tag{10}$$

with boundary conditions

$$u = 0,\ \frac{\partial h}{\partial r} = 0,\ \frac{\partial \Gamma}{\partial r} = 0 \text{ at } r = 0, \tag{11}$$

and undisturbed far field condition

$$u = 0,\ h = 1,\ \Gamma = 0 \text{ at } r = \infty. \tag{12}$$

3 Numerical scheme for the IME regime thin film equations

The IME regime was also discretised using a centered finite difference, analogous to sections 1, 2. However, an explicit method was used for the temporal discretisation as there was no capillary pressure term (so no third order spatial derivatives present) and since there is a viscous stress term. A sponge layer was not needed due to the presence of a dissipative term (viscous extensional stress), which meant that only a moderately sized domain was needed to avoid spurious reflections from the numerical boundaries.

The key difference to the IMC regime is the fact that the size of the front region (referred to as region II as in the main text) decreases like $t^{-\frac{1}{2}}$. Thus, it was advantageous to take a mesh with spatial adaptivity. Temporal adaptivity was not considered, though such considerations would make the computation cheaper. The IME equations that we wish to solve numerically are given by

$$\frac{\partial u}{\partial t} = -u\frac{\partial u}{\partial r} - \frac{2}{h}\frac{\partial \Gamma}{\partial r} + \frac{4}{Re}\frac{1}{h}\left(\frac{\partial}{\partial r}\left(\frac{h}{r}\frac{\partial}{\partial r}(ru)\right) - \frac{1}{2}\frac{u}{r}\frac{\partial h}{\partial r}\right), \tag{13a}$$

$$\frac{\partial h}{\partial t} = -\frac{1}{r}\frac{\partial}{\partial r}\left(ruh\right), \tag{13b}$$

$$\frac{\partial \Gamma}{\partial t} = -\frac{1}{r}\frac{\partial}{\partial r}\left(ru\Gamma\right). \tag{13c}$$

with initial and boundary conditions

$$u = 0,\ h = 1,\ \Gamma = e^{-r^2} \text{ at } t = 0, \tag{14}$$

$$u = 0,\ \frac{\partial h}{\partial r} = 0,\ \frac{\partial \Gamma}{\partial r} = 0 \text{ at } r = 0, \tag{15}$$

$$u = 0,\ h = 1,\ \Gamma = 0 \text{ at } r = \infty. \tag{16}$$

3.1 Numerical scheme

3.1.1 Choice of spatial grid

The grid was taken to be $[0, L]$ with $L = 200$, which was sufficiently large to capture the behaviour of u, h, Γ for the times considered (the simulation was run until $h_{\min} = 10^{-3}$). The gridpoints were chosen adaptively. In particular, the simulation was run on Basilisk [3] and the adaptive mesh grid algorithm in the `grid/bitree.h` file was used. For details, see [1]. In particular, there are three control parameters. The first two are the minimum and maximum level of grid refinement. A grid at level l would have be $L/2^l$ in length. The final parameter is the refinement criterion, referred to as ζ by van Hooft et al. [1]. The value $\zeta > 0$ is the estimated error of refinement. When ζ is smaller, the grid is refined more and vice versa.

3.1.2 Choice of numerical solver

An explicit Euler scheme with centered finite difference is considered. At the origin $r = 0$, Dirichlet condition was used to set $u = 0$ and Neumann conditions are used to set $\frac{\partial h}{\partial r} = \frac{\partial \Gamma}{\partial r} = 0$. The details of the boundary at the right are irrelevant as the domain is sufficiently large.

3.1.3 Summary of parameters for numerics

There are 4 parameters in total (3 spatial, 1 temporal). See Table 5.

Parameter	Description
$l_{\min}$	Minimum level of spatial resolution [section 1.1.1]
$l_{\max}$	Maximum level of spatial resolution [section 3.1.1]
ζ	(spatial) Refinement criterion [see section 3.1.1]
Δt	timestep (uniform) [see section 3.1.2]

Table 5: Summary of parameters for the numerical scheme for the IME regime

3.2 Numerical convergence

The convergence of the numerical scheme is verified for the three key physical predictions: $h_{\min}$, r_f, and h upto $rt^{-\frac{1}{2}}$. The numerical schemes are run until $h_{\min} \approx 10^{-3}$. Explicitly, the code is run upto $t = 750$ ($Re = 1$), $t = 400$ ($Re = 4$), and $t = 300$ ($Re = 10$).

It is found that the following set of parameters are well converged. These parameters are referred to as the base case. All the simulations took under 130 CPU hours on a single core.

- $Re = 1$: $\Delta t = 2 \times 10^{-6}$, $l_{\min} = 10$, $l_{\max} = 16$, $\zeta = 10^{-4}$
- $Re = 4$: $\Delta t = 10^{-6}$, $l_{\min} = 10$, $l_{\max} = 18$, $\zeta = 10^{-4}$
- $Re = 10$: $\Delta t = 6 \times 10^{-7}$, $l_{\min} = 10$, $l_{\max} = 19$, $\zeta = 10^{-4}$

In order to check convergence, we refined or coarsened each of the numerical parameters and compare the results. The summary of the cases are given in table 6. The comparisons for minimum thickness $h_{\min}$, front location r_f, and thickness profile h at end time are shown in figure 4. Thus, the base case parameters have converged.

	minlevel	maxlevel	ζ	time
$Re = 1$	$l_{\min} = 11$	$l_{\max} = 17$, $\Delta t = 10^{-6}$	$\zeta = 10^{-5}$	$\Delta t = 10^{-6}$
$Re = 4$	$l_{\min} = 11$	$l_{\max} = 17$	$\zeta = 10^{-5}$	$\Delta t = 5 \times 10^{-7}$
$Re = 10$	$l_{\min} = 11$	$l_{\max} = 18$	$\zeta = 10^{-5}$	$\Delta t = 3 \times 10^{-7}$

Table 6: Summary of parameters changes with respect to the base case for the IME regime (see section 3.2) used to check for convergence. For example, $Re = 1$ for $l_{\min}$ refinement uses the parameters $l_{\min} = 11$, $l_{\max} = 16$, $\zeta = 10^{-4}$, $\Delta t = 10^{-6}$.

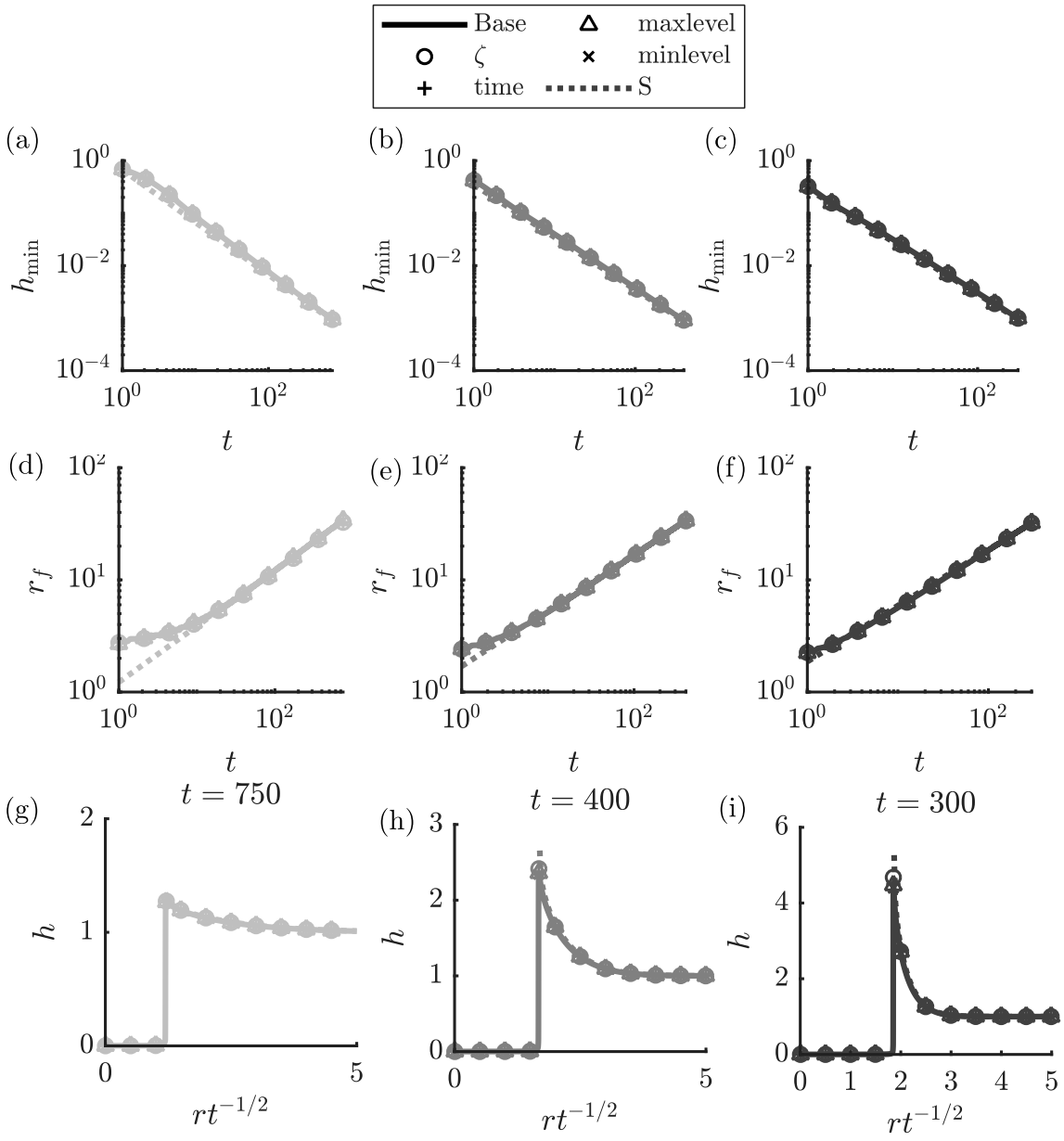

Figure 4: Convergence check for the IME regime. (a,b,c) Comparison of the base case (solid) with the different cases (hollow symbols) as in table 6, for minimum thickness $h_{\min}$. (d,e,f) Analogous comparisons for front location r_f. (g,h,i) Analogous comparisons for the thickness profile at the end of the simulation. In all figures, the similarity solution prediction (S) are shown as dotted lines.

4 Numerical scheme for the IMCE regime thin film equations

The IMCE equations that we wish to numerically integrate are given by the following:

$$\frac{\partial u}{\partial t} = -u\frac{\partial u}{\partial r} - \frac{2}{h}\frac{\partial \Gamma}{\partial r} + \frac{1}{2\mathcal{M}}\frac{\partial}{\partial r}\left(\frac{1}{r}\frac{\partial}{\partial r}\left(r\frac{\partial h}{\partial r}\right)\right) + \frac{4}{Re}\frac{1}{h}\left(\frac{\partial}{\partial r}\left(\frac{h}{r}\frac{\partial}{\partial r}(ru)\right) - \frac{1}{2}\frac{u}{r}\frac{\partial h}{\partial r}\right), \quad (17a)$$

$$\frac{\partial h}{\partial t} = -\frac{1}{r}\frac{\partial}{\partial r}\left(ruh\right), \quad (17b)$$

$$\frac{\partial \Gamma}{\partial t} = -\frac{1}{r}\frac{\partial}{\partial r}\left(ru\Gamma\right). \quad (17c)$$

with initial and boundary conditions:

$$u = 0,\ h = 1,\ \Gamma = e^{-r^2} \text{ at } t = 0, \quad (18)$$

$$u = 0,\ \frac{\partial h}{\partial r} = 0,\ \frac{\partial \Gamma}{\partial r} = 0 \text{ at } r = 0, \quad (19)$$

$$u = 0,\ h = 1,\ \Gamma = 0 \text{ at } r = \infty. \quad (20)$$

4.1 Numerical scheme

4.1.1 Choice of spatial grid

The grid was taken to be $[0, L]$ with $L = 500$, which was sufficiently large to capture the behaviour of u, h, Γ for the times considered (the simulation was run until $t = 1000$). The gridpoints are uniformly spaced with $r_i = \frac{\Delta}{2} + i\Delta$ for $i = 0, ..., N-1$ where $\Delta = L/N$. The discretisation is centered and hence is the same as (5) but with the capillary stress term and viscous extensional stress term.

4.1.2 Choice of numerical solver

Crank-Nicolson with uniform timestep Δt is considered. At the origin $r = 0$, Dirichlet condition was used to set $u = 0$ and Neumann conditions are used to set $\frac{\partial h}{\partial r} = \frac{\partial \Gamma}{\partial r} = 0$. Again, the details of the boundary at the right are irrelevant.

4.1.3 Summary of parameters for numerics

There are only 2 parameters in total (1 spatial, 1 temporal). Namely, the number of gridpoints N and timestep Δt.

4.2 Numerical convergence

For all $\mathcal{M}, Re$, we consider the following three cases to show numerical convergence. The base case takes under about 10 CPU hours on a single core, and the other two cases take under about 50 CPU hours on a single core.

- base case: $N = 10^4$, $\Delta t = 0.2$.
- Δt: $N = 10^4$, $\Delta t = 0.1$.
- N: $N = 2 \times 10^4$, $\Delta t = 0.1$.

Figure 5 verifies numerical convergence for the minimum thickness $h_{\min}$ and front location r_f. Figure 6 verifies numerical convergence of the thickness profiles at time $t = 1000$. Thus, we can see that there is good numerical convergence.

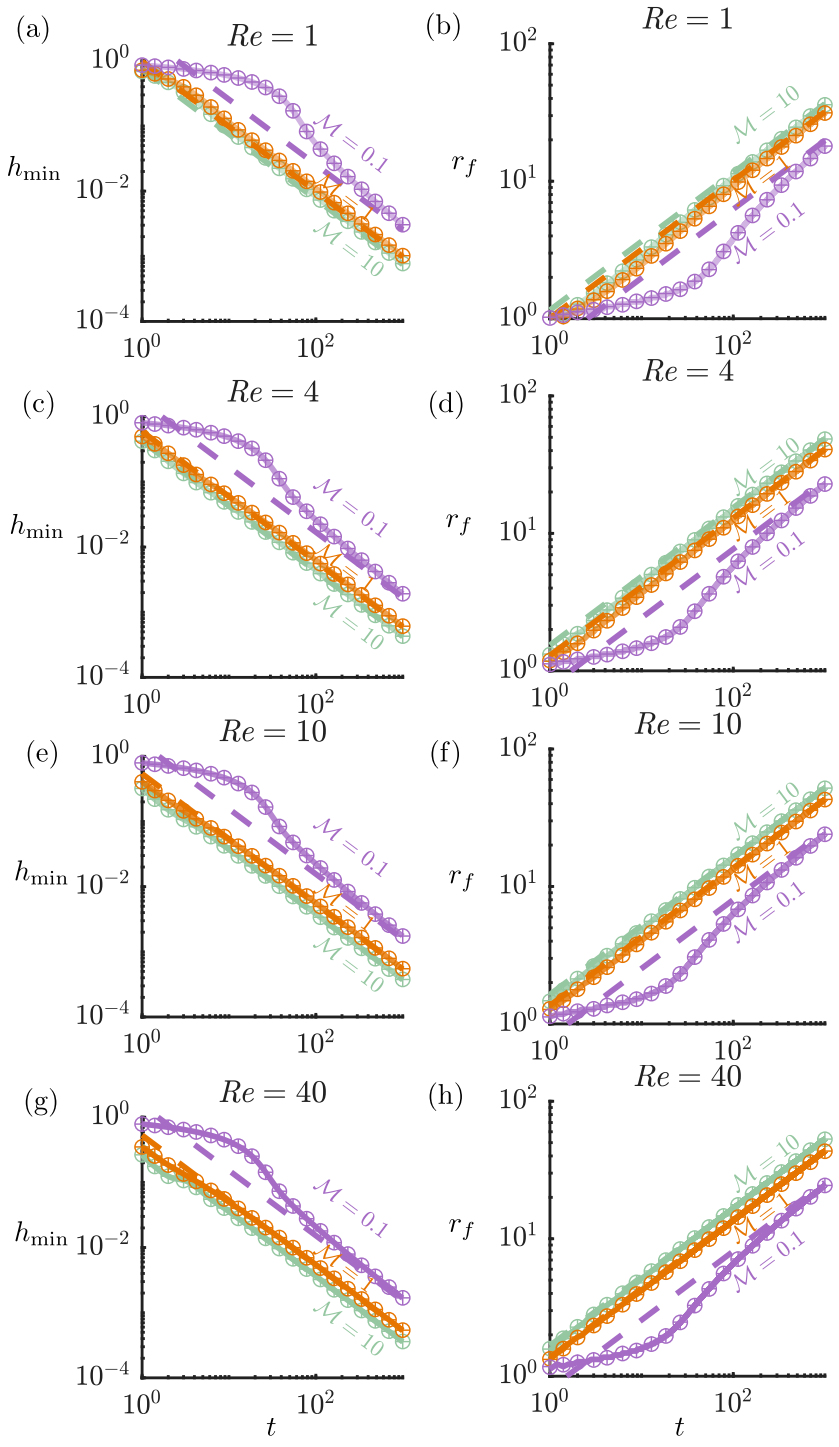

Figure 5: Numerical convergence checks for minimum thickness $h_{\min}$ (a,c,e,f) and front location r_f (b,d,f,h) for $Re = 1, 4, 10, 40$. Solid curves denotes the numerical result of the base case, and the symbols show the result of refining N (circle) and Δt (cross). The dashed curve shows the similarity solution prediction. Colors denote values of parameter $\mathcal{M}$ ($\mathcal{M} = 0.1$: purple, $\mathcal{M} = 1$: orange, $\mathcal{M} = 10$: blue-green).

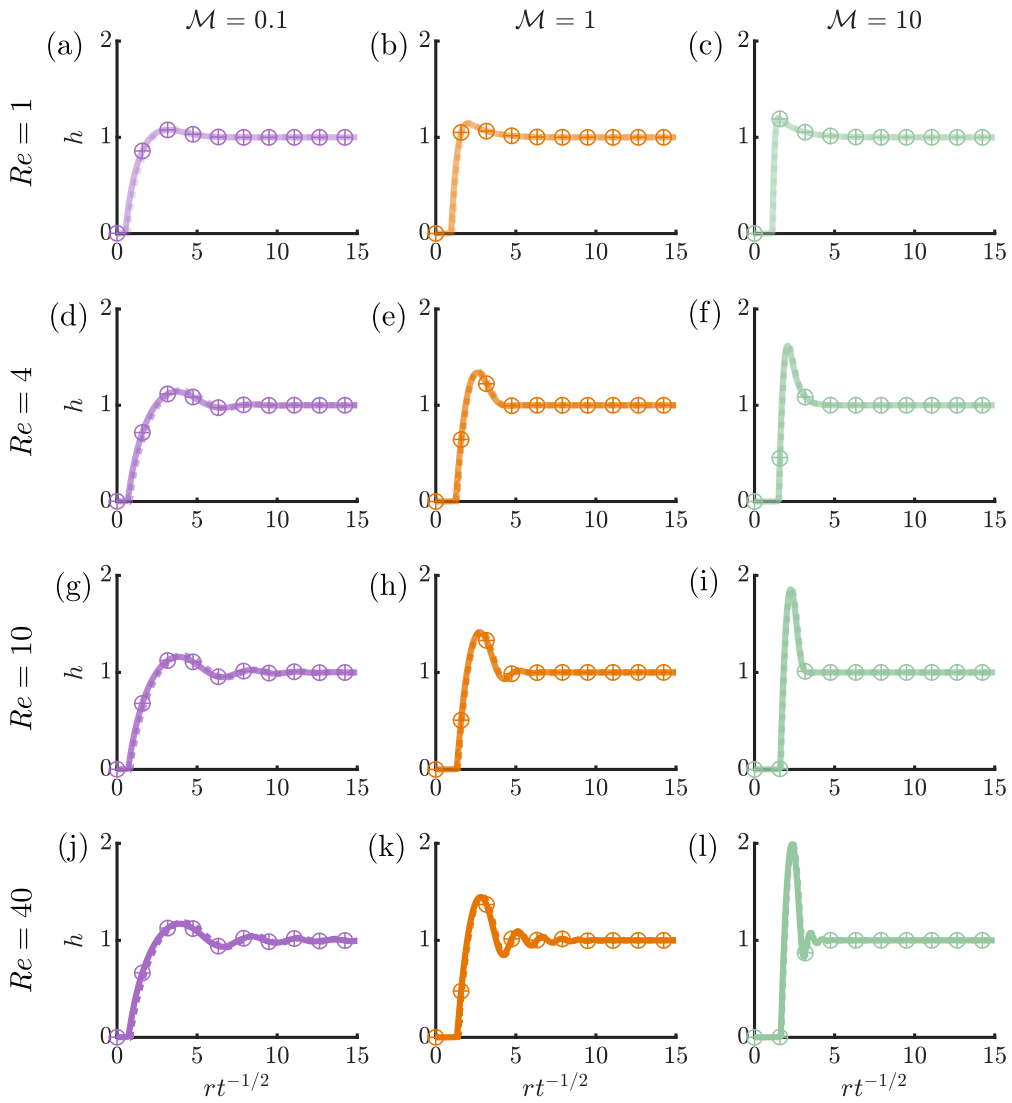

Figure 6: Numerical convergence checks for late time ($t = 1000$) thickness profiles h against $rt^{-\frac{1}{2}}$ where r is the radial coordinate and t denotes time. Solid curves gives the base case parameters, and the symbols show the result of refining N (circle) and Δt (cross). The dashed curve shows the similarity solution prediction. The cases shown are $\mathcal{M}, Re = [0.1, 1, 10] \times [1, 4, 10, 40]$.

References

[1] J. A. van Hooft, S. Popinet, C. C. van Heerwaarden, S. J. A. van der Linden, S. R. de Roode, and B. J. H. van de Wiel. "Towards adaptive grids for atmospheric boundary-layer simulations". In: *Boundary-layer meteorology* 167 (2018), pp. 421–443.

[2] J. Eshima, H. A. Stone, and L. Deike. "Precursors of Thin Film Rupture: Similarity Solution of Surfactant-Driven, Inertial Capillary Waves". In: *Physical Review Letters* 134.21 (2025), p. 214002.

[3] S. Popinet and collaborators. *Basilisk*. `http://basilisk.fr`. 2013–2025.